Sequential heat release (SHR): an innovative approach for the control of curing profiles during composite processing based on dual-curing systems

Maria Romero, Xavier Fernández-Francos,* Xavier Ramis

Thermodynamics Laboratory, ETSEIB, Universitat Politècnica de Catalunya, Av. Diagonal 647, 08028 Barcelona, Spain

*Corresponding author: xavier.fernandez@upc.edu

Phone: +34 934017955

Fax: +34 934017389

This article has been accepted for publication and undergone full peer review but has not been through the copyediting, typesetting, pagination and proofreading process which may lead to differences between this version and the Version of Record. Please cite this article as doi: 10.1002/pi.5743

Abstract

The sequential heat release (SHR) taking place in dual-curing systems can facilitate thermal management and control of conversion and temperature gradients during processing of thick composite parts, hence reducing the appearance of internal stresses that compromise the quality of processed parts. This concept is demonstrated in this work by means of numerical simulation of conversion and temperature profiles during processing of an off-stoichiometric thiol-epoxy dual-curable system. The simulated processing scenario is the curing stage during resin transfer moulding processing (RTM) (i.e. after injection or infusion), assuming one-dimensional heat transfer across the thickness of the composite part. The kinetics of both polymerization stages of the dual-curing system and thermophysical properties needed for the simulations have been determined using thermal analysis techniques and suitable phenomenological models. The simulations show that SHR makes it possible to reach a a stable and uniform intermediate material after completion of the first polymerization process, and enables a better control of the subsequent crosslinking taking place during the second polymerization process due to the lower remaining exothermicity. A simple optimization of curing cycles for composite parts of different thickness has been performed on the basis of quality-time criteria, producing results that are very close to the Pareto-optimal front obtained by genetic algorithm optimization procedures.

Keywords: Thermosetting resin; Dual curing; Cure behaviour; Numerical Analysis; Resin Transfer Moulding (RTM)

1 Introduction

The control of temperature gradients and uniformity of conversion profiles during processing of composite parts based on thermosetting resins is essential for the quality of the processed parts.[1-4] The high exothermicity of curing reactions of most thermosetting systems, coupled with their poor heat dissipation capabilities, may lead to the presence of undesired temperature overshoots and non-uniform conversion profiles that can result in the appearance of residual stresses that can provoke defects such as warpage, cracking and delamination. Thermal- and chemically-induced shrinkage during processing, especially once the material has gelled and is therefore developing mechanical strength, are the main responsible for this. If the temperature reached within the bulk of the part is too high, thermal degradation might even occur. Staged curing of prepreg stacks[5] or processing in multiple temperature stages[3] are possible strategies. Control of temperature and conversion profiles can be achieved by defining complex temperature programmes involving a number of heating and cooling steps that are optimized following diverse numerical procedures.[1-3, 6-9] Optimization criteria are usually based on controlling exothermic peaks,[3] uniform conversion profiles[1] or multi-objective functions including multiple effects such as internal stress calculations.[2, 9]

Dual-curing thermosetting formulations that combine two different polymerization reactions are an interesting alternative to conventional curing systems due to the possibility of controlling the curing sequence, the extent of curing in the intermediate stage, and the intermediate and final network structure and properties.[10] This is achieved by means of choosing selective initiators and/or triggers for each reaction and by simply changing the composition and structure of the monomers participating in each reaction. A general representation of dual-curing processing is shown in Scheme 1. These features make them attractive for a number of advanced applications, but the control of the curing sequence is also valuable for different processing scenarios such as multi-stage processing (i.e. B-staging) or the curing of thick composite parts, because of the possibility of stopping or slowing down the process once the first polymerization process is over, and of controlling the molecular or network structure in this intermediate state. This is a clear advantage with respect to conventional B-stageable formulations that have to be tightly controlled in terms of processing time-temperature in order to obtain the desired partially cured structure and therefore ensure successful application.[11] Indeed, the sequential heat release (SHR) produced by the separation of the two polymerization processes can facilitate thermal

management and control during processing of composite parts, because dissipation of heat that is being released in two well-defined and separate stages is easier than in a simple curing process. In consequence, a highly uniform and stable intermediate state can be reached within the bulk of the composite part at the end of the first polymerization process. Due to the lower remaining exothermicity and concentration of reactive groups, subsequent activation and occurrence of the second polymerization reaction can take place in a more controlled way, with little temperature and conversion gradients. The possibility of tailoring the network/molecular structure of the intermediate material, makes it possible to place gelation at the very end of the first polymerization stage or within the second stage, so that the intermediate material is only lightly crosslinked or still liquid-like. Therefore, the subsequent crosslinking process takes place (almost) entirely during the second polymerization stage, where the conversion and temperature profiles are more uniform, hence minimizing the formation of internal stresses. In summary, dual-curing makes it possible to achieve, with chemistry, what is achieved after mathematical optimization[1, 2] in conventional curing systems.

Scheme 1

In order to test the feasibility of this concept, the processing of composite parts is analyzed making use of off-stoichiometric thiol-epoxy formulations with excess epoxy groups and using tertiary amine initiators,[12] recently developed by our research group. Thiol-epoxy polymerization in presence of a nucleophilic tertiary amine as initiator takes place at a fast rate at low temperature and, once finished, the excess epoxy groups can homopolymerize at a slower rate and higher temperatures. Scheme 1 outlines the two different polymerization processes taking place in the dual-curing system. This curing system has manifold advantages: only one initiator is required to activate both reactions, a wide range of tertiary amine initiators are available, formulations can be safely prepared due to the slow activation of the curing process, and it can be used dual-curing applications where UV irradiation is not feasible. Intermediate materials with properties ranging from viscoelastic liquid to lightly crosslinked structures can be easily designed by means of changing the monomer feed ratio and their structure.[12, 13] It makes sense to choose a dual-curing formulation that does not gel in the first curing stage, so that a stable liquid-like intermediate material is obtained, and crosslinking takes place entirely in the second curing stage in a more controlled way (see Scheme 1).

In this paper, we test this concept using a a dual-curable formulation based on diglycidyl ether of Bisphenol A (DG) and Trimethylolpropane tris (3-mercaptopropionate) (S3) with an excess of epoxy groups, using 1-methylimidazole (1MI) as anionic initiator. The processing of composite parts based on this system was simulated by a finite differences method assuming unidimensional heat transfer. Curing kinetics and thermophysical properties of the dual-curing system were determined experimentally, while suitable models were used to determine the effective properties of composite parts. In order to illustrate the viability of the concept, a number of different processing scenarios are studied, and methods for the optimization of the cure cycle, based on uniform conversion and reduced processing time criteria, are discussed.

2 Materials and methods

2.1 Materials

Diglycidyl ether of bisphenol A (DG) with an epoxy equivalent weight of 172-176 g/eq (Aldrich) was dried at 80 ºC under vacuum for 2 hours and stored in a dessicator prior to use. Trimethylolpropane tris (3-mercaptopropionate) (S3) and 1-methylimidazole (1MI) from Sigma Aldrich have been used as received.

Table 1

A set of mixtures using DG as epoxy monomer and with different ratios *r* of thiol groups with respect to epoxy groups were prepared, adding 1 phr (parts per hundred of the total mixture) of 1MI with respect to the total mixture as catalyst. The samples were quickly stirred with a spatula and analyzed immediately after. Table 1 shows the composition of the different formulations. The formulations have been coded as DGS3-r, where *r* is the thiol:epoxy equivalent ratio. It should be mentioned that the thiol equivalent weight was assumed to be the theoretical value of 132.85 g/eq for the calculation of the composition, although the supplier reports a purity of 98 % for this product.

Fully cured samples for characterization were prepared by casting and curing in a convection oven following a stepped curing procedure consisting of a first stage at 50 ºC for one hour followed by a heating at 120 ºC and kept at that temperature for one extra hour.

2.2 Characterization techniques

Curing kinetics

Two differential scanning calorimeters Mettler DSC821e and DSC822e (equipped with a robotic arm TSO801RO and using liquid nitrogen), both calibrated with indium standards, were used to study the isothermal and nonisothermal curing of the different formulations at different temperatures and heating rates. Samples of ca 2-10 mg (higher mass for lower heating rates and temperatures) were placed inside an aluminum pan with a pierced lid and were inserted into the preheated oven before analysis, under nitrogen atmosphere.

The calorimetric degree of conversion was determined as $x = \Delta h / \Delta h_{total}$, where Δh is the reaction heat released up to a time t and Δh_{total} is the total reaction heat evolved. The calorimetric reaction rate was determined as $dx/dt = (dh/dt)/\Delta h_{total}$, where dh/dt is the heat flow.

For the dual-curing formulation DGS3-0.5, the first and second curing processes were analyzed individually, For the first curing process, isothermal experiments were stopped when it was observed that the first reaction process was finished. Dynamic experiments were performed up to completion of the whole process, but the curves were only analyzed up to the end of the first curing process. For the second curing process, a set of samples were precured at 80 ºC in the DSC and stopped inmediately after the first process was finished, and they were analyzed afterwards under different isothermal or nonisothermal conditions. As a result of this stepped analysis, parameters Δh_1, x_1 and dx_1/dt were obtained for the first curing process, and Δh_2, x_2 and dx_2/dt for the second curing process.

In the case of the simple system DGS3-1, the epoxy conversion was assumed to be directly proportional to the calorimetric signal $x_{epoxy} = x$. In the case of the dual system DGS3-0.5, the epoxy conversion was calculated as $x_{epoxy} = 0.5 \cdot x_1 + 0.5 \cdot x_2$. The maximum epoxy conversion at the end of the first curing reaction (before the second reaction is activated) is therefore $x_{epoxy} = 0.5$.

Glass transition temperatures

The calorimeter Mettler DSC822e was also used to determine the glass-transition temperature of the uncured, partially cured and fully cured samples, that is, T_{g0}, T_{gint} and $T_{g\infty}$ respectively. The samples were analyzed at 10 ºC/min and the glass transition temperature was determined as the halfway point in the heat capacity step. The heat capacity steps of the uncured, partially cured and fully cured samples (Δc_{p0}, Δc_{pint} and $\Delta c_{p\infty}$ respectively) were also determined. The fully cured samples were heated twice at 10 ºC/min, the first time to erase the thermal history and the second one to determine the glass transition temperature. The evolution of the glass transition temperature with the degree of conversion can be approximated as[14]

$$ln\, T_g(x) = \frac{(1-x)\cdot ln\, T_{g0} + \left(\Delta c_{p\infty}/\Delta c_{p0}\right)\cdot x \cdot ln\, T_{g\infty}}{(1-x) + \left(\Delta c_{p\infty}/\Delta c_{p0}\right)\cdot x} \qquad \textbf{(1)}$$

For a single curing process, this expression makes use of parameters T_{g0}, $T_{g\infty}$ and the ratio $\Delta c_{p\infty}/\Delta c_{p0}$, which are measured before and after curing. In the case of a dual curing process, this expression might be applied to the first part of the curing process (making use of T_{g0}, T_{gint} and the ratio $\Delta c_{pint}/\Delta c_{p0}$ instead, measured before and after the first curing stage) and to the second part of the curing process (making use of T_{gint}, $T_{g\infty}$ and the ratio $\Delta c_{p\infty}/\Delta c_{pint}$ instead, measured before and after the second curing stage). This approach was successfully used in the analysis of the $T_g(x)$ relationship of a an off-stoichiometric amine-epoxy dual-curing system.[15] This expression was used to determine whether the curing system is in the relaxed state ($T > T_g(x)$) or not during processing.

Gel point determination

A thermo-mechanical analyzer Mettler TMA SDTA840 was used to determine the conversion at the gel point following a procedure previously discussed.[16, 17] A silanized glass fiber disc ca. 5 mm in diameter was impregnated with the liquid formulation and sandwiched between two thin aluminum discs. The sample was heated up from 25 to 250 ºC at 2 ºC/min, and subject to an oscillatory force of 0.005-0.01 N with an oscillation frequency of 0.083 Hz (dynamic load thermo-mechanical analysis mode, DLTMA). The gel point temperature was taken as the onset in the decrease of the oscillation amplitude measured by the probe. The conversion at the gel point was determined from the gel point temperature and a dynamic curing experiment in the

DSC at the same heating rate. The sample temperatures measured by the thermocouple below the sample in the TMA analyzer, and that measured by the cell in the DSC, were used to ensure accuracy of the measurement.

Specific heat capacity

The specific heat capacity (C_p) was determined using the calorimeter Mettler DSC822e using the methodology described in the methods DIN 51007. Alumina (Al_2O_3) was used as reference for the specific heat capacity.[18]

For the DGS3-1 formulation, the C_p of the uncured (liquid) and fully cured material was determined. Assuming that in the simulations the material would be in the relaxed state, we can calculate the C_p of partially cured materials depending on temperature T and degree of conversion x as:

$$C_p(x,T) = (1-x)\cdot C_{p0}(T) + x\cdot C_{p\infty}(T) \quad \textbf{(2)}$$

Where the temperature-dependence of the specific heat capacity was approximated to $C_p = a + b\cdot T$.

For the dual-curable DGS3-0.5 formulation, we determined the C_p of the uncured (liquid), intermediate and fully cured materials. Assuming that the material would be in the relaxed state, we can calculate the C_p depending on temperature T and degree of conversion x_1 (first process) and x_2 (second process) as:

$$C_p(x_1,x_2,T) = \left[(1-x_1)\cdot C_{p0}(T) + x_1\cdot C_{p,int}(T)\right]\cdot(1-x_2) + x_2\cdot C_{p\infty}(T) \quad \textbf{(3)}$$

For this expression to be valid, there should be a controlled curing sequence and therefore good separation between processes, as is commonly observed in off-stoichiometric thiol-epoxy systems.[12, 13, 19]

More complex expressions can be found in the literature describing the effect of vitrification on C_p.[3, 20] However, the model presented in this section should suffice to describe the temperature and conversion dependence of the C_p as long as it is verified that the material is at a temperature sufficiently above $T_g(x)$.

Density

The density of the uncured formulations at room temperature, T_0, was determined by picnometry. The density at room temperature of the fully cured DGS3-1 and DGS3-0.5 materials, and the partially cured DGS3-0.5 materials were determined by the flotation method in a KBr solution and picnometry.

The density of cured samples at temperatures T other than room temperature were estimated by thermomechanical analysis using a Mettler TMA SDTA840, heating the cured samples at 5 K/min under nitrogen atmosphere. Assuming isotropy, the density at a temperature was T estimated as:

$$\rho_\infty(T) = \frac{\rho_\infty(T_0)}{v(T)/v(T_0)} = \frac{\rho_\infty(T_0)}{(L(T)/L(T_0))^3} \quad \textbf{(4)}$$

Where $L(T)$ and $L(T_0)$ are the sample thickness at temperatures T and T_0, respectively. The expressions were approximated $L(T)/L(T_0) = a + b \cdot T$ above the glass transition temperature, and $L(T)/L(T_0) = a + b \cdot T + c \cdot T^2$ below the glass transition temperature.[21]

The density of liquid uncured formulations DGS3-1 and DGS3-0.5, and of partially cured formulation DGS3-0.5 (liquid-like in the present case) at temperatures T other than room temperature was estimated using the approximation of Van Krevelen for oligomers or polymers above their glass transition.[22, 23]

$$\rho(T) = \rho(T_0) \cdot \left(1 - 0.000625 \cdot (T - T_0)\right) \quad \textbf{(5)}$$

It is assumed that, for the DGS3-1 formulation the density $\rho_r(x, T)$, at a given x and T, can be determined assuming additivity of specific volumes of the cured and uncured fractions:

$$\rho_r(x, T) = \left[(1 - x) \cdot \frac{1}{\rho_0(T)} + x \cdot \frac{1}{\rho_\infty(T)}\right]^{-1} \quad \textbf{(6)}$$

For the dual-curable DGS3-0.5 formulation, we determined the density of the uncured (liquid), intermediate and fully cured materials. Assuming that the material would be in the relaxed state, we calculated the C_p depending on temperature T and degree of conversion x_1 (first process) and x_2 (second process) as:

$$\rho_r(x_1, x_2, T) = \left[\left[(1 - x_1) \cdot \frac{1}{\rho_0(T)} + x_1 \cdot \frac{1}{\rho_{int}(T)}\right] \cdot (1 - x_2) + x_2 \cdot \frac{1}{\rho_\infty(T)}\right]^{-1} \quad (7)$$

Although resin density changes can be neglected for modelling purposes,[1, 4] in other cases thermally- or chemically- induced specific volume or density changes in the resin are considered in order to determine the overall change of thickness of composite parts or the pressure build-up in constant-volume systems.[24] However, once gelation has occurred, the effect is more complex and includes also the effect of mechanical stresses. For simplification purposes, we will consider only the thermally- or chemically- induced density changes of the resin, and that subsequent density changes only produce a change in the composite thickness.

Thermal conductivity

The measurements of the thermal conductivity were made using the transient hot bridge method (Linseis, GmbH, THB-100, Selb, Germany) and a Kapton Hot Point sensor (Linseis). The THB-100 instrument applies a controlled heating power, typically 50 mW, to the sensor, sandwiched between two pieces of the sample to be analyzed, and measures the resulting temperature change in the sample as a function of time. The thermal conductivity, λ, can be determined from the extrapolated temperature rise of the sample at infinite time. Details on the fundamentals of the transient hot bridge method can be found in the literature.[25]

Two fully cured samples samples (of DGS3-1 or DGS3-0.5 formulations) were used for these measurements. The surfaces (12 x 25 mm^2) of each sample were carefully polished manually using emery paper, in order to give flat and smooth surfaces for contact with the Kapton sensor. The sensor was clamped between the two flat faces of the two samples, using a manual screw-actuated press. The measurements were carried out only at room temperature.

It is acknowledged that the thermal conductivity of thermosetting resins and composites can vary with the degre of conversion and temperature.[1, 3, 20, 24, 26] Neglecting this effect might be a source of error in the simulations.

2.3 Kinetic modelling

The experimental rate curves were fitted to a modified multi-term Kamal model inspired in the models employed by other authors[24, 27] shown in eq. (8),

$$\frac{dx}{dt} = f(x,T) = \frac{dx}{dt} = \sum_{i=1}^{k} k_i \cdot x^{m_i} \cdot (1-x)^{n_i} \tag{8}$$

$$k_i = k_{0,i} \cdot exp(-E_i/R \cdot T)$$

where m_i and n_i are the exponents of each autocatalytic function, and k_i is an Arrhenius kinetic constant for each autocatalytic process. The number of adjustable parameters is high, as it includes E_i and $k_{0,i}$ for the different k_is and the reaction orders m_i and n_i for each autocatalytic function. We determined the model parameters by multivariate nonlinear regression, with the following error function to be minimized:

$$error = \frac{1}{n}\sum \frac{\left|\left(\frac{dx}{dt}\right)_{exp} - \left(\frac{dx}{dt}\right)_{calc}\right|}{\left(\frac{dx}{dt}\right)_{exp}} \tag{9}$$

where $(dx/dt)_{exp}$ and $(dx/dt)_{calc}$ are the experimentally measured, and the calculated reaction rates, respectively, at the same degree of conversion, and n are the number of calculated and measured points used for the fitting. Given that the fitting is performed on reaction rate with respect to conversion rather than on conversion with respect to temperature/time, the effect of an induction period i.e. due to the slow activation of the reaction not be properly accounted for. In addition, in the above expression there is no reaction rate at the beginning of the reaction. Therefore, integration would only be valid above a certain threshold value of conversion.

One can define an induction time t_{ind} as the time to reach a given threshold conversion, x_{ind}, using the following expression based on the integration of rate a generic rate equation $dx/dt = k(T) \cdot f(x)$ and assuming the validity of isoconversional hypotheses during the induction period:[28]

$$g(x_{ind}) = \int_0^{x_{ind}} \frac{dx}{f(x)} = k_{0,ind} \cdot \int_0^{t_{ind}} exp\left(-\frac{E_{ind}}{R} \cdot \frac{1}{T}\right) \cdot dt \tag{10}$$

In this expresion, $g(x_{ind})$ is the integral form of the kinetic model function $f(x)$ at the induction fractional conversion x_{ind}, and E_{ind} is the activation energy corresponding to the induction period. The parameters $\ln\left(g(x_{ind})/k_{0,ind}\right)$ and E_{ind} are assumed to be constant during the induction period. This expression is, implicitly, the basis for other expressions used in the literature for the modelling of induction periods.[2]

Under isothermal conditions, integration of eq. (10) leads to:

$$\ln t_{ind} = \ln\left(\frac{g(x_{ind})}{k_{0,ind}}\right) + \frac{E_{ind}}{R} \cdot \frac{1}{T} \quad (11)$$

Under constant heating rate experiments, one can make use of the approximation of the temperature integral as:

$$\frac{g(x_{ind})}{k_{0,ind}} = \frac{1}{\beta} \cdot \frac{E_{ind}}{R} \cdot p(\varphi) \quad (12)$$

where β is the heating rate, $\varphi = E_{ind}/R \cdot T_{ind}$, T_{ind} is the temperature at the defined induction fractional conversion, and $p(\varphi)$ is the 3rd order Senum-Yang approximation[29, 30] of the temperature integral. A determination of $g(x_{ind})/k_{0,ind}$ and E_{ind} from both isothermal and constant heating rate experiments can therefore be made by nonlinear regression techniques using the above expressions. In this work, we chose $x_{ind} = 0.01$.

Starting from eq. (10), we can consider that, for $x < x_{ind}$, the conversion is given by

$$x \approx x_{ind} \cdot \frac{\int_0^t exp(-E_{ind}/R \cdot T) \cdot dt}{g(x_{ind})/k_{0,ind}} \quad (13)$$

Therefore, the reaction rate dx/dt, for $x < x_{ind}$ would be given by:

$$\frac{dx}{dt} \approx x_{ind} \cdot \frac{exp(-E_{ind}/R \cdot T)}{g(x_{ind})/k_{0,ind}} \quad (14)$$

For $x > x_{ind}$,we can consider that the reaction rate dx/dt is represented correctly by eq. (8).

For the simple system DGS3-1, a single set of kinetic parameters was determined. However, for the dual system, two separate sets of kinetic parameters were determined, for the first process (with conversion x_1) and for the second proces (with conversion x_2).

It should be noted that the effect of vitrification during curing is implicitly neglected in this choice of reaction model. This simplification should be valid as long as it can be verified that the material is at a temperature sufficiently above $T_g(x)$ throughout processing.

2.4 Simulation model

The chosen scenario was the simulation of composite parts processed by resin transfer molding, focusing only on the curing stage. The simulations were performed assuming unidimensional

heat transfer in the transverse direction of the composite part, as commonly done in the literature.[1, 2, 4, 21] The constitutive equation for the heat dissipation and generation of heat is:

$$\frac{d}{dz}\left(\lambda \cdot \frac{\mathrm{d}T}{\mathrm{dz}}\right) + \dot{Q}_{gen} = \rho \cdot c_p \cdot \frac{dT}{dt} \tag{15}$$

Where λ, ρ and c_p are the effective thermal conductivity, density and specific heat capacity of the composite part, respectively, the extent of conversion of the reacting system x, the resin volume fraction ϕ_r and the temperature T. Note that there is also the implicit assumption that the resistance to heat transfer between the resin and the filler is negligible. $\dot{Q}_{gen}$ is the generation of heat due to the curing process. The transverse direction is indicated by z. The generation term can also be expressed as

$$\dot{Q}_{gen} = \frac{dh}{dt} \cdot \phi_r \cdot \rho_r \tag{16}$$

, where dh/dt is the heat flow released by the reaction per mass unit of resin, ϕ_r is the volume fraction of the resin, and ρ_r is the density of the resin.

In the case of a single curing process, the heat released can be expressed as

$$\frac{dh}{dt} = \Delta h \cdot \frac{dx}{dt} \tag{17}$$

, where Δh is the reaction heat and dx/dt is the reaction rate depending on x and T. In the case of a dual system, the expression would be

$$\frac{dh}{dt} = \Delta h_1 \cdot \frac{dx_1}{dt} + \Delta h_2 \cdot \frac{dx_2}{dt} \tag{18}$$

, where Δh_1, dx_1/dt are the reaction heat and reaction rate for the first process, and Δh_2, dx_2/dt are the reaction heat and reaction rate for the second process, respectively. Although the different curing processes in the dual system DGS3-0.5 are considered to be sequential,[12, 19] we allowed for some overlapping, so that the calculation of dx_2/dt, corresponding to the second curing process, could start when $x_1 > 0.99$.

The effective thermophysical properties of the composite parts were calculated using models available in the literature for glass fiber reinforced composites. All the properties are dependent on the filler glass content, and in this work we have assumed a filler volume fraction $\phi_f = 0.5$, similar to other composite systems reported in the literature.[2]

For the transverse thermal conductivity λ, we used the following model:[1]

$$\lambda = \lambda_r \cdot \frac{(1+\phi_f)\cdot\lambda_f + (1-\phi_f)\cdot\lambda_r}{(1-\phi_f)\cdot\lambda_f + (1+\phi_f)\cdot\lambda_r} \quad (19)$$

In the above expression, λ_r and λ_f are the thermal conductivities of the resin and the filler, respectively, and ϕ_f is the filler volume fraction, with $\phi_f = 1 - \phi_r$. The value of λ_r was obtained experimentally, while it is assumed that $\lambda_f = 0.9\ W/m \cdot K$.

For the effective specific heat capacity we used a weighed average as follows[24]

$$c_p = w_r \cdot c_{pr} + (1 - w_r) \cdot c_{pf} \quad (20)$$

, where c_{pr} and c_{pf} are the specific heat capacities of the resin and the filler, respectively, and w_r is the mass fraction of the resin. c_{pr} was calculated from experimental measurements, and it was assumed that $c_{pf} = 700\ J/kg \cdot K$. The mass fraction of the resin was calculated as

$$w_r = \frac{\phi_r \cdot \rho_r}{\phi_r \cdot \rho_r + \phi_f \cdot \rho_f} \quad (21)$$

, where ρ_r and ρ_f are the densities of the resin and the filler, respectively. ρ_r was calculated from experimental measurements and it is assumed that $\rho_f = 2200\ kg/m^3$.

The effective density of the composite ρ was calculated as:

$$\rho = \phi_r \cdot \rho_r + +\phi_f \cdot \rho_f \quad (22)$$

The simulated geometry is represented in Figure 1(a). A composite part with thickness L is cured between two tooling parts with controlled and equal program temperature T_{prog}. Assuming symmetry, only half of the composite part needs to be simulated, from the adiabatic central node to the surface in contact with the tooling, with a thickness $L/2$. In the present work, the curing of composite parts with total thickness L equal to 8, 16 and 24 mm was simulated. The system was discretized in nodes with thickness Δz (except the adiabatic central node, at $z = 0$, with thickness $\Delta z/2$). The curing schedule is given by the evolution of the tooling temperature T_{prog}. Figure 1(b) shows a typical programming curve, consisting of different steps.

Figure 1

Boundary conditions, assuming simmetry and convective heat transfer with the environment, were defined as follows:

$$z = 0 \Longrightarrow \frac{dT}{dz} = 0 \tag{23}$$

$$z = \frac{L}{2} \Longrightarrow q_{L/2} = -\lambda \cdot \left.\frac{dT}{dz}\right|_{L/2} = h_{contact} \cdot \left(T_{L/2} - T_{prog}\right)$$

In the preceding expression, $h_{contact}$ represents the resistance to heat transfer from the point within the tooling at which the temperature T_{prog} is set to the interface between the composite part and the tooling, $T_{L/2}$ is the composite temperature at the boundary and $q_{L/2}$ is the heat flow across the boundary between the composite part and the tooling. However, since the surface temperature $T_{L/2}$ was not evaluated, the boundary condition was set making use of the nodal temperature corresponding to the n[th] node of the composite part, T_n (in the center of the node, as seen in Figure 1(a)), as

$$q_{L/2} = h \cdot \left(T_n - T_{prog}\right) \tag{24}$$

$$h = \left(\frac{\Delta z}{\lambda} + \frac{1}{h_{contact}}\right)^{-1}$$

, where $\Delta z/\lambda$ corresponds to the resistance to heat transfer between the boundary and the center of the n[th] node. The higher $h_{contact}$, the closer is the temperature at the n[th] node to T_{prog}. The value of $h_{contact}$ was arbitrarily set to a value of 1500 W/m^{2}K, giving values of the characteristic Bi number of the composite part ($Bi = h_{contact} \cdot (L/2)/\lambda$) within the range of 10-50 for the analyzed composite parts. This value is comparable to those explored in some works [4] but somewhat lower than that used in other published works [6]. Values of h or $h_{contact}$ are not generally reported [1, 2, 20], while in some cases it is assumed that temperature at the boundary is equal to the programmed temperature [24]. For applications such as autoclave processing, lower heat transfer coefficients within the range of 30-100 W/m^{2}K should be used.[3]

The discretized expressions for the nodal temperatures were integrated numerically using the implicit, 2[nd] order Crank-Nicolson method. The reaction rate equations for the nodal conversions were integrated explicitly using the 2[nd] order Runge-Kutta method. The coupling of temperature-conversion profiles, and the thermal and conversion dependence of material properties, make it necessary to evaluate the reaction rate and material properties at the temperature and conversion after the integration step. In order to overcome this, a fixed-point

iteration was performed, with updating of the material properties and reaction rate at every iteration step, until convergence of the calculated temperature and conversion at each integration step. A predictor of the integration step was obtained from the explicit nodal temperature and conversion expressions. Integration was performed using home-made algorithms in MATLAB.

2.5 Cure cycle optimization

Criteria for optimization of cure cycles are usually based on controlling exothermic peaks,[3, 9] uniform conversion profiles[1] or multi-objective fitness functions that include these effects and also internal stress calculations.[2, 9] Evolutionary or genetic algorithms are popular,[7, 9] although other optimization methods can be followed.[1, 6] The concept of Pareto-optimal front can also be used to obtain a more complete view on the trade-off between processing time and quality of the processed part.[3]

In the present work, we defined a quality criterion consisting in minimizing cure gradients after the gel point, in a similar way to other works.[1, 9] First of all, we calculated the average epoxy conversion $\bar{x}$ and the standard deviation S_x at any time t as

$$\bar{x} = \frac{1}{p} \cdot \sum_{j=1}^{p} x_{epoxy,j} \qquad S_x = \left[\frac{1}{p-1} \cdot \sum_{j=1}^{p} \left(x_{epoxy,j} - \bar{x} \right)^2 \right]^{\frac{1}{2}} \tag{25}$$

, where p is the number of nodes. The quality function $S_{x,mean}$ was therefore defined as:

$$S_{x,mean} = \left[\sum_{x_{epoxy,gel}}^{\bar{x}=0.98} \left(\bar{x} - x_{epoxy,gel} \right) \cdot S_{x_j} \right] \Bigg/ \left[\sum_{x_{epoxy,gel}}^{\bar{x}=0.98} \left(\bar{x} - x_{epoxy,gel} \right) \right] \tag{26}$$

For a uniform conversion profile, $S_{x,mean}$ should be as low as possible. The factor $\left(\bar{x} - x_{epoxy,gel} \right)$ is used to give more weight to the final stages of the crosslinking process, where the effect of increasing mechanical properties and developing internal stresses due to thermal strain and chemical shrinkage strain should be more relevant.

As a second optimization criterion we have chosen to minimize the cure cycle time, t_{cycle}, defined as the time needed to reach $\bar{x} = 0.99$. As shown in Figure 1(b), the cooling down to room temperature was excluded from the cycle.

In the basic curing cycle (see Figure 1(b)), the program temperature T_{prog} increases at 5 ºC/min up to a dwell temperature T_{dwell}, where it remains for a certain period t_{dwell}. A second heating takes place, at a heating rate β and up to a final temperature of 120 ºC, where it remains until the cure is completed ($\bar{x} = 0.99$). This basic curing cycle can be modified to include a preheating step in order to accelerate the start of the reaction. In this case, the program temperature T_{prog} increases at 5 ºC/min up to the preheat temperature $T_{preheat}$, it then decreases at 5 ºC/min to the dwell temperature T_{dwell}, and the rest of the curing program is identical.

A first optimization was performed starting from trial-and-error simulations and exploration of the decision space, making use of the different adjustable parameters. The dwell temperature T_{dwell} was set tentatively by trial-and-error in order to avoid an exceedengly large temperature overshoot during the first polymerization process, and to ensure the composite part reaches a uniform conversion after the end of the first polymerization reaction. In the case of the basic cycle, as adjustment parameters we chose the dwell time (t_{dwell}) and the second heating rate (β), evaluated at discrete intervals. The heating rate β was limited to 5 ºC/min, although higher heating rates are allowed in composite processing [1]. In the case of the modified program, we included also the preheat temperature $T_{preheat}$. It was assumed that the optimum heating rate corresponded to the same determined for the basic cycle, so that optimization was carried out using as adjustment parameters t_{dwell} and $T_{preheat}$, evaluated at discrete intervals. This optimization process was computed in MATLAB using home-made algorithms.

By this procedure, which combines an intuitive-based approach with numerical optimization, we avoid full exploration of the decision space[3, 9] and therefore save some computation time, but we acknowledge it produces a single optimum solution that is dependent on the tentative selection of the dwell temperature T_{dwell} and the discretization of the decision space.

In order to examine the trade-off between quality and processing time, we determined the Pareto-optimal front,[3] confronting $log_{10}(S_{x,mean})$ and t_{cycle}. This optimization process was carried out using the MATLAB built-in genetic algorithms for multiobjective optimization.

Table 2 shows the parameters used in the genetic algorithm (all other parameters were set to default values). The parameters T_{dwell}, t_{dwell}, $\Delta T_{preheat}$ $(= T_{preheat} - T_{dwell})$ and β were used as variables and were subject to upper and lower constraints. The results of the previous optimization were compared with the Pareto-optimal front.

Table 2

3 Results and discussion

3.1 Preliminary characterization

Figure 2 compares the dynamic curing at 10 ºC/min of stoichiometric DGS3-1 and off-stoichiometric DGS3-0.5 formulations. It can be clearly seen that, in the case of the DGS3-1 formulation, the curing process is simple, taking place in a single step, corresponding to the nucleophile-initiated thiol-epoxy polymerization.[12, 19, 31] However, in the case of DGS3-0.5 formulation, the curing takes place in two well-separated steps: the first one is the thiol-epoxy polymerization and the second one, that takes place once the thiol groups are exhausted, the homopolymerization of the epoxy groups in excess.[12, 19] Both reactions are depicted in Scheme 1 (right hand side). The reaction mechanisms of nucleophile-initiated thiol-epoxy polymerization and epoxy homopolymerization have been recently discussed in detail elsewhere.[12, 19, 31-33] Because the kinetics of the second process are much slower than the first one, it has been possible to develop recently a new family of dual-curable thermosetting materials[12] that have found, so far, an application in shape-memory devices.[13, 34, 35]

Figure 2

The sequential heat release (SHR) taking place during curing of DGS3-0.5 formulation evidences the interest in the use of such dual-curing systems for the processing of composite parts. In more specific terms, this interest arises from: (1) the different reactivity of both curing stages, already seen in Figure 2, (2) the possibility of carrying out the first part of the curing process at temperatures as low as room temperature,[31] (3) the presence of a significant induction period, related with the slow initiation of the process,[19, 31] before the thiol-epoxy polymerization is activated, and (4) the possibility of tailoring the molecular or network structure at the end of the first curing stage.[12]

To begin with, this long induction period is highly useful for processing purposes, in that there is plenty time for infusion of the resin into the moulded part, with no appreciable change in properties. At 30 ºC, this induction period can be within the range of 1-2 h for the DGS3-0.5 formulation,[31] and the initial viscosity for the stoichiometric formulation is lower than 0.5 Pa·s.[36] In addition, in thiol-epoxy off-stoichiometric formulations the network structure at the end of the first processing stage can be easily tailored just by changing the thiol-epoxy ratio.[12] In the case of the DGS3-0.5, we verified experimentally that gelation and subsequent crosslinking take place during the second curing stage.[13] This is of crucial importance, because it does not matter if the first curing stage is not uniform at all, because the system is still liquid-like at the end of it. We only have to make sure that we are able to reach a uniform and stable intermediate state throughout the thickness of the composite part at some point, before the second reaction is activated. Given that part of the heat has already been released during the first curing stage, the control of the second stage of the process would be much easier, therefore making it possible to have more uniform conversion profiles during this stage and, therefore, uniform crosslinking, in a similar way to other works reported in the literature.[1, 2]

Table 3 shows the results of the preliminary thermal characterization DGS3-1 and DGS3-0.5 formulations. One can notice some remarkable differences between both formulations. To begin with, formulation DGS3-0.5 is, overall, more exothermic than DGS3-1 (472 versus 419 J/g), respectively. However, in the DGS3-0.5 case the heat released in the first curing stage, Δh_1, is about 60 % of the total heat released,[12] which is due to the fact that thiol-epoxy polymerization releases about 130 kJ/ee[12, 36] while epoxy homopolymerization releases only about 100 kJ/ee.[37-39] Indeed, the calculated values in kJ/ee for the simple curing process of DGS3-1 and both curing stages of DGS3-0.5 (see Table 3) agree well with the reference values of 130 kJ/ee for the thiol-epoxy addition[12, 36] and 100 kJ/ee for the epoxy homopolymerization.[37-39] Therefore, it can be assumed safely that quantitative conversion of epoxy groups takes place in any case. For the DGS3-1 the $T_{g\infty}$ is equal to 34 ºC but for the DGS3-0.5 system it is equal to 79 ºC, as reported previously,[12, 13] because of the contribution of the tighter network structure of the homopolymerized epoxy. In previous works[12, 13] we reported that this increase in $T_{g\infty}$ was accompanied by an increase in relaxed modulus due to the higher crosslink density caused by the homopolymerization of the excess epoxy groups in the DGS3-0.5 formulation. The intermediate glass transition temperature of the DGS3-0.5, T_{gint}, is equal to 9 ºC, which indicates that the intermediate material is in the relaxed state at room temperature. It is

interesting to note that for both DGS3-1 and DGS3-0.5 there is a clear decrease in the values of the heat capacity step before and after cure, Δc_{p0} and $\Delta c_{p\infty}$ respectively, in agreement with the change in T_g for crosslinking systems. In contrast, in the first curing stage of DGS3-0.5 the values of Δc_{p0} and Δc_{pint} are almost equal. Taking the ratio $\Delta c_{pint}/\Delta c_{p0}$ as a parameter that is descriptive of the evolution of the glass transition temperature during the first curing reaction,[14, 21, 40] this suggests that in the first curing stage there is a linear increase in T_g with respect to conversion. Such linearity indicates that the system is in the liquid state all throughout the first stage of the curing process,[40] in agreement with our previous experimental observations.[13] Indeed, following the methodology explained in section 2.2, we verified that gelation occurred in the second stage of the curing process[13] We determined a gel point conversion in the second stage $x_{2,gel} = 0.25$, which is equivalent to say that $x_{epoxy,gel} = 0.63$ (because the first process is complete, so that $x_1 = 1$). The conversion at the gel point for the DGS3-1 formulation was equal to $x_{epoxy,gel} = 0.80$. Given that the mechanism of the thiol-epoxy reaction is complex and involves a series of initiation, propagation and regeneration steps,[19, 31] theoretical gel-point predictions can only be made starting from a mechanism-based kinetic model that takes into consideration the concentration of all the relevant reactive species, and use it in a suitable network build-up model for step-wise processes, based on structural fragments.[21] However, predictions can also be made, with a reasonable accuracy, assuming that the initiator is acting like a thiol co-monomer with a functionality of 1 and use the expressions for ideal step-wise behaviour[21] (note that it affects the effective co-monomer functionality and ratio of reagents). For the DGS3-1 formulation this results in a theoretical gel point conversion of 0.73-0.74 (slightly above the theoretical conversion of 0.71 assuming only a trifunctional thiol crosslinker[12]), and for the DGS3-0.5 formulation the model predicts that the system is very close to gelation at the end of the first curing stage. However, given that the experimental gel-point conversion of DGS3-1 formulation is even higher and that gelation of DGS3-0.5 takes place well within the second curing process, it is hypothesized that the occurrence of intramolecular cyclization is the responsible for such deviations from ideality, as reported previously.[13]

Table 3

Figure 3 shows the rate curves corresponding to the first and second curing processes of DGS3-0.5 formulation under isothermal conditions. First of all, it can be clearly appreciated the difference in reactivity between the first and second process. At 80 ºC, the reaction peak in the

first process is about 30 times higher than in the second process. At temperatures as low as 30 ºC, in the first process it can be appreciated an induction period of about 90 minutes that indicates that there should be enough time to inject the sample in the mould cavity before the reaction starts. It is also observed that the first process has a very strong autocatalytic behaviour, as reported previously,[19] therefore there is a serious risk of temperature runaway if the programmed temperature is too high. Given that crosslinking would take place entirely in the second curing stage and that the first curing process is much faster and more exothermic than the second one, the key point to ensure uniform crosslinking during processing of the composite part will be to control the exothermicity during the first curing process, so that the second curing process does not start. However, it may be allowed some advancement of second curing reaction providing gelation has not taken place yet.

Figure 3

The curing kinetics of DGS3-1 and both curing processes of DGS3-0.5 have been analyzed using the methods explained in section 2.3. The results of the kinetic modelling of all processes are shown in Table 4 for DGS3-1, and Table 5 and Table 6 for DGS3-0.5. In order to illustrate the suitability of the methodology and the kinetic models employed, the upper graph in Figure 4 compares the experimental and predicted rate curves of the first curing process of DGS3-0.5 under isothermal conditions. Taking into account experimental uncertainty, especially considering the high reactivity of these systems at low temperature, the quality of the fit is remarkable. Given that the model is purely phenomenological, the values of the model parameters are not connected with the reaction mechanism. The activation energies of the different processes agreed well with the values obtained using the isoconversional methodology and previously reported data.[12]

Table 7 shows that the relative errors associated with the fitting of the rate curves is relatively low, around 5 % (note that the relative error at the beginning and the end of the curves is usually larger due to the low reaction rate). The error associated with the induction time is also low for the DGS3-1 system and for the first process of the DGS3-0.5 system, but it is significantly higher for the second process of the DGS3-0.5 system. This is because one of the experimental curves had a very large error due to experimental uncertainty at the beginning of the rate curves and that there is no induction at all (see lower graph of Figure 3). The lower graph in Figure 4 shows that the isothermal conversion corresponding the first curing process of DGS3-0.5 could

be properly predicted. The agreement between calculated and experimental isotherms was comparable in the other cases. In conclusion, the employed kinetic methodology produced results that could be used to simulate the curing process with confidence.

Figure 4

Table 4

Table 5

Table 6

Table 7

We also measured and estimated (using suitable models) the thermophysical properties relevant for the simulation of the processing of DGS3-1 and DGS3-0.5 formulations, reported in Table 8. The values of c_p are always around 1700-2000 $kJ/kg \cdot K$ (up to temperatures of, say, 120 ºC), with a positive temperature dependence and within the typical ranges for other epoxy systems reported in the literature,[1] although higher values have been reported.[41] The measured values of the thermal conductivity λ_r are also similar to other values reported in the literature for epoxy resins.[1, 20, 41] However, we could only measure the value at room temperature of the cured resin, so that the effect of the degree of cure and the temperature is neglected and is therefore a source of error in the simulations.

Table 8

3.2 Simulation results

The scenario that is simulated is the processing of composite parts by resin transfer moulding (RTM), focusing only on the curing stage. Given that thiol-epoxy systems have a long induction period at room temperature[31] and that initial viscosity at room temperature is low,[36] we consider that the injection can be decoupled from the curing process.[2] In order to simplify the scenario, we will neglect the injection time. In all the simulations we carried out, we assumed a fiber glass volume fraction of 50 %, similar to other composite systems.[2]

Initial simulations

First of all, we compared the curing of a 8 mm thick composite part using DGS3-1 and DGS3-0.5 formulations. Following the programming scheme in Figure 1(b), the temperature programming consisted in a firts heating step from 25 to 70 ºC at 5 ºC/min, followed by a dwell at that temperature for a certain period of time and, if needed, finally heated up at 5 ºC/min up to 120 ºC, where they were left to react until completion. The $x-t$ and $T-t$ profiles during processing are shown in Figure 5.

Figure 5

The curing of the simple formulation, DGS3-1, starts shortly after the composite reaches the temperature of 70 ºC and, due to the autocatalytic characteristics of the reaction and the high reaction rate, a large temperature overshoot occurs in the center of the composite part leading to very fast completion of the reaction, and diverging conversion across the thickness of the part, meaning that the crosslinking process ($x_{epoxy,gel} = 0.80$) is far from being uniform. In the case of formulation DGS3-0.5, there is an earlier temperature overshoot because the reaction can start earlier [19], leading to fast conversion rate in the center of the part and completion of the first reaction process (occurring at $x_{epoxy} = 0.5$) . However, given that the second reaction is much slower, the final conversion after the temperature overshoot does not exceed $x_{epoxy} = 0.55$, which is only slightly higher than the conversion in the part surface, and still lower than the conversion at the gel point $x_{epoxy,gel} = 0.63$. If the composite part is kept for a longer time at this temperature, the second reaction process could take place slowly. However, upon heating up to 120 ºC, it is observed that the reaction becomes faster in the part surface and the conversion profile gets gradually narrower, producing an almost uniform crosslinking process.

The conversion and temperature profiles across the thickness of the composite part are shown in Figure 6 and Figure 7 for the formulations DGS3-1 (simple curing) and DGS3-0.5 (dual curing), respectively. Figure 6 evidences the strong conversion and temperture gradients throughout the composite part taking place during the whole curing process when DGS3-1 is used. This is of special relevance when gelation is reached (at $x_{epoxy} = 0.8$), leading to significant chemically and thermally induced internal stresses. In contrast, for DGS3-0.5 Figure 7 shows only relevant temperature and conversion gradients before the end of the first curing process, taking place and $x_{epoxy} = 0.5$. At higher degrees of conversion, during the second polymerization process, the

temperature and conversion profiles are rather flat throughout the composite thickness. Because gelation takes place at $x_{epoxy} = 0.63$, crosslinking takes place entirely during the second polymerization process and in cosnequence the formation chemically and thermally induced internal stresses is minimized.

Figure 6

Figure 7

Note that this result is not qualitatively different from those shown in other references [1, 2] after numerical optimization of the temperature programme. In the present case, no effort has been made to optimize the curing schedule yet, other than choosing a suitable dwell temperature. This is mainly a consequence of the unique features of the dual-curing system employed: 1) the occurrence of two consecutive reaction processes with clearly different kinetics, and 2) the absence of gelation after completion of the first reaction process. Hereinafter, therefore, all the simulations are carried out using the dual-curing formulation DGS3-0.5.

Successful application of the sequential heat release (SHR) concept in system under study requires effective dissipation of the heat released during the first polymerization stage, in order to avoid premature activation of the second polymerization process. Figure 8 shows the effect of changing the dwell temperature from 60 to 80 ºC. It can be seen that, at 80 ºC, the temperature overshoot is so large that the second polymerization process is already activated and the material already gels in the inner layers of the composite part, while in the outer layers the temperature is closer to the prescribed temperature programme. The conversion and temperature gradients during the crosslinking process are significant, therefore producing a non-uniform crosslinking process and, eventually, higher internal stresses. However, at 60 ºC, the temperature overshoot is sufficiently small, so that the degree of conversion gets highly uniform across the thickness of the sample at the end of it, around $x_{epoxy} = 0.5$. Upon heating, the conversion and temperature profiles during the second curing process are highly uniform. Table 9 shows the values of the quality parameter $S_{x,mean}$ for these three simulations (entries 1, 2 and 3 for 80, 70 and 60 ºC respectively). It is apparent that the uniformity in the case of the simulation at 60 ºC is excellent, with a value of 10^{-3}. At 70 ºC the uniformity is quite acceptable, with a value of $6 \cdot 10^{-3}$, while at 80 ºC the resulting parameter is about $2 \cdot 10^{-2}$. It should be noted that, given the uniformity shown in the process simulated at 60 ºC, it could also be possible to

stop the second curing process by cooling down at almost any time in order to obtain a part with a controlled extent of cure, as in the literature [1].

Figure 8

Table 9

Therefore, choice of a suitable dwell temperature seems to be a critical factor in the control of the extent of cure at the end of the first curing stage and the uniformity of the conversion and temperature profiles during the crosslinking process taking place in the second curing stage. This is of especial importance when considering the processing of thicker composite parts, where the dissipation of heat is more difficult and therefore the occurrence of uncontrolled temperature overshoots is more likely. In consequence, we decided to analyze what would be the situation for composite parts with thicknesses of 16 and 24 mm instead, and with the same fibre volume fraction $\phi_f = 0.5$.

On the basis of preliminary trial-and-error simulations, we found that the dwell temperature for 16 mm samples had to be further reduced in order to prevent uncontrolled temperature runaway in the first temperature stage. A tentative curing programme consisting in a firts heating step from 25 to 45 ºC at 5 ºC/min, followed by a dwell at that temperature that was extended until the temperature overshoot was over. Then the programmed temperature was increased at 5 ºC/min up to 120 ºC, and it was kept at this temperature until completion of the reaction. When the sample thickness was increased to 24 mm, the dwell temperature was reduced to 35 ºC in order to control the temperature and conversion profiles during curing. Figure 9 compares these new simulations with the previous simulation of the curing of a 8 mm thick part with a dwell temperature of 60 ºC. Due to the need of decreasing the first dwell temperature, it is clearly seen that the curing process is logically extended to longer times. The first exothermic peak also increases with sample thickness due to the accumulation of heat, while the uniformity of the curing and temperature profiles after gelation is also affected. Entries 3, 4 and 5 of Table 9 show that the quality of the processed part decreases with increasing thickness (increasing values of $S_{x,mean}$) and that the curing cycle of the 24 mm part (entry 5) is more than twice longer than that of the 8 mm part (entry 3).

Figure 9

In all these preliminary simulations, it was verified (making use of eq. (1) and the data in Table 3) that the curing temperature was higher than the glass transition temperature $T_g(x)$, so the effect of vitrification on kinetics and other thermophysical properties could be safely neglected.

Optimization of processing parameters

The trial-and error adjustment of T_{dwell} led to fairly satisfactory results, as could be expected from the dual-curing nature of DGS3-0.5 formulation. However, the quality of the results decreased noticeably with increasing composite thickness. Therefore, we decided to see if we could optimize the curing programme by adjusting the dwell time t_{dwell} and the heating rate β. We carried out a number of simulations by changing systematically t_{dwell} and β, and determined the quality $S_{x,mean}$. We then selected the t_{dwell} and β so that we obtained the best quality with reasonable curing times. In order to explain the procedure and the results, we will focus on the processing of 16 mm composite parts.

Figure 10 shows the results of this analysis. It can be observed that at too short dwell times the crosslinking process is highly non-uniform (high $S_{x,mean}$) because of the activation of the first reaction during the second heating step, at too high temperatures, leading to a temperature runaway producing the uncontrolled activation of the second reaction. However, at higher dwell times the uniformity clearly improves because the exothermic peak corresponding to the first reaction takes place at the dwell temperature and in a controlled manner. At all the heating rates there is a clear optimum at a given value of t_{dwell}. The quality improves (lower $S_{x,mean}$) by increasing β up to an optimum heating rate of 3-3.5 ºC/min. At low heating rates, the heating and temperature profile is highly uniform but, due to the existence of an initial conversion gap after completion of the first polymerization, conversion is higher in the inner layers throughout the crosslinking process. At higher heating rates, temperature increases faster in the outer layers, leading to faster cure and higher conversion than in the inner layers, leading also to nonuniform crosslinking. Moreover, at the optimum heating rate of 3-3.5 ºC/min the optimum region is broader, so that a further increase in t_{dwell} does not produce a significant increase in $S_{x,mean}$.

Figure 10

An optimum curing schedule was therefore selected with $\beta = 3.5\ ºC/min$ and $t_{dwell} = 35\ min$. The total curing cycle was reduced to 97.7 minutes and the quality of the processed

part improved, with a resulting value of $S_{x,mean} \approx 0.0028$ (lower than the value shown in entry 4, Table 9). The original and modified curing cycles for the 16 mm part are represented in Figure 11. It can can be seen that the heating starts before the temperature overshoot is over, when the first curing reaction is already over in the center of the composite part but before completion in the surface layer. The conversion gradient gradually becomes narrower and the crosslinking process, after gelation takes place, is quite uniform. The temperature profiles are also quite uniform, with a small overshoot in the center at the end of the heating process that is concomitantly reduced after this optimization.

Figure 11

Concerning the optimum value of t_{dwell} (see Figure 10), it can be observed that extended dwell period at the optimum heating rate produce only a limited increase in $S_{x,mean}$ and therefore a decrease in uniformity during the crosslinking. This is of special importance in terms of quality because, in the event that the formulation was left prepared for a while and therefore a certain degree of pre-curing was present in the sample (still within the induction period, though), this would result in an advance of the temperature overshoot. This would be equivalent to extend the dwell time, so that the heating might start when the overshoot was over but, at the optimum heating rate, the effect would be very limited. The consequences would be more dramatic if the curing programme had been optimized at a heating rate of 5 ºC/min (see Figure 10).

Figure 11 also shows that there is a significant induction period before the reaction starts, so that it would be desirable to shorten the curing cycle by a preheating at a higher temperature before the dwell at the desired temperature. Inspired by the results in the literature,[2, 9] we defined a preheating at 5 ºC/min up to a peak temperature, followed by a cooling down at 5 ºC/min down to the chosen dwell temperature. We carried out an optimization by optimizing the peak temperature and the dwell time, while keeping constant the optimum heating rate which, for the 16 mm composite part and dwell temperature of 45 ºC, was 3.5 ºC/min. The results of this optimization are shown in Figure 12. It can be seen that, for all the peak temperatures analyzed, there is an optimum dwell time leading to a minimum value of $S_{x,mean}$. Increasing this peak temperature led to somewhat higher values of $S_{x,mean}$ but, overall, within the same range. The dwell time was also considerably shortened with increasing peak temperature. Therefore, in order to optimize the curing time, we decided to choose the maximum peak temperature of 70

ºC (at higher temperatures such as 75 ºC the values of $S_{x,mean}$ were higher), and the optimum value of t_{dwell}.

Figure 12

The main parameters of this shortened curing cycle are shown in Table 10, entry 2. If we compare this with the previously optimized cycle, we observe a significant shortening of the cycle time, from 98 to 85 minutes, while not compromising the uniformity of the crosslinking process, with a value of $S_{x,mean}$ equal to 0.0028, as in the previous optimization. Comparison between the optimized cycle (Table 10, entry 2) and the original cycle (Table 9, entry 4) evidence the effectiveness of this optimization procedure.

Table 10

In addition, we did the whole optimization procedure for a composite part of 24 mm and 8 mm. For the 24 mm part, we maintained the dwell temperature of 35 ºC, the heating rate was optimized to 2.5 ºC/min and the dwell time and the preheating temperature were finally optimized. In Table 10, entry 3, it can be seen that the resulting quality is very high, with a a value of $S_{x,mean}$ of 0.0042. The overall cycle time is higher than for 16 mm composite parts (Table 10, entry 2) because, logically, the dwell temperature needs to be smaller in order to control the temperature overshoot. For the 8 mm thick sample, a dwell temperature of 60 ºC, a heating rate of 4 ºC/min and a preheat temperature of 70 ºC (Table 10, entry 1) were chosen. The curing time is shorter and the quality is higher because it is easier to control the release and dissipation of heat with a lower thickness, so that a higher dwell temperature, shorter dwell time and higher heating rate can be used.

We represented all these new curing cycles in Figure 13. It is observed that, due to the preheating and the thermal lag between the center and the surface of the composite part, the center temperature does not reach back the programmed dwell temperature before the exothermic peak is observed. Moreover, due to the shortening of the dwell period, the subsequent heating process starts within the exothermic peak, very close the temperature peak. Although there may be a conversion gap as a result of the temperature overshoot, the resulting temperature and conversion profiles become highly uniform after the gel point. As seen in Figure 13 and Table 10, higher thickness demands longer processing times and decreases the uniformity of the crosslinking process but, overall, the results are highly satisfactory.

Again, we checked that, in these simulations, the curing temperature was higher than the glass transition temperature $T_g(x)$, so the effect of vitrification on kinetics and other thermophysical properties could be safely neglected. The results of the check were satisfactory except for some extreme cases during optimization of 24 mm thick samples. An exceedingly large value of $T_{preheat}$ (such as 75 ºC) would produce a temperature runaway leading to higher degrees of cure in the center of the part; if the part was allowed to cool down completely to T_{dwell} before the second heating started, it could be found that $T < T_g(x)$ within the inner layers of the composite part for a short period of time. Although that would have an effect on the thermophysical properties and kinetics, the overall effect on the thermal simulation would be minor. No problems were found for the optimization of 8 and 16 mm parts and, in fact, all the optimized programmes in Table 10 and Figure 13 fulfilled the condition $T > T_g(x)$.

Figure 13

The above results evidence that, owing to the unique nature of these dual-curing systems, it is possible and very easy to design curing schedules with controlled temperature and conversion profiles during crosslinking. A simplified procedure can thus be defined: (1) a dwell temperature has to be chosen so that the temperature overshoot due to the exothermicity and fast reaction of the first curing process is controlled and leads to a reduced conversion gap across the composite thickness, (2) a safe heating rate and a tentative dwell time are optimized so as to maximize the uniformity along the crosslinking stage and (3) a preheat temperature and final dwell time are optimized to reduce the cure cycle without compromising the quality.

The sensitivity of $S_{x,mean}$ to processing parameters such as $T_{preheat}$ and t_{dwell} (see Figure 10 and Figure 12) suggests that it would be safer, in terms of quality, to limit $T_{preheat}$ and, especially, extend t_{dwell}. Exceedingly high $T_{preheat}$ would lead to an uncontrolled temperature runaway in the preheating step, and a too short t_{dwell} would lead to the same during the second heating. This is of special importance in the case of thicker composite parts. In addition, the curing of thiol-epoxy formulations is highly sensitive to preparation, so that the time elapsed between mixing and curing (or analysisis) is also a critical factor.[31] A pre-reacted sample would have a shorter induction during processing, so that a temperature runaway might occur during preheating, following the same optimized curing schedule obtained for a fresh sample. In that respect, limiting $T_{preheat}$ makes even more sense. Therefore, sample preparation and mold

injection/infusion time should be carefully controlled, and this effect should be incorporated in the simulation and optimization.

As noted in the literature, the space and time distribution of conversion, temperature and stresses are not independent from each other.[1] However, optimization based on the control of conversion profiles or internal stresses may lead to somewhat different solutions,[9] due to the complex effect of temperature and conversion profiles on the appearance of internal stresses during processing.[2, 9] Moreover, the appearance of internal stresses is even more sensitive to processing parameters than the conversion-temperature profiles, which makes it advisable to take them into consideration in the optimization function.[9] In the present case, the control of temperature is more relevant to the temperature overshoot taking place during the first polymerization process, while control of conversion is more linked to the second polymerization process, where crosslinking takes place. The trial-and-error choice of the first dwell temperature ensured a proper control of the first temperature overshoot, so that a uniform conversion throughout the part thickness could be reached. The subsequent optimization of processing parameters, based on the criterion of obtaining a uniform conversion profile after the gel point, leads to the presence of a small temperature overshoot during crosslinking, at the end of the heating ramp (see Figure 13), but it is significantly lower than in the preliminary simulations before optimization (see Figure 9). This might have some adverse effect in terms of internal stresses, but it is within acceptable ranges reported in the literature.[2, 9] Regardless of whether the optimization criterion includes the generation of internal stresses or not, the application of the sequential heat release (SHR) concept, based on the use of dual-curing systems such as the one studied in this work, would still be valid.

Pareto optimal front

In the preceding optimization procedure, the decision space was limited to exploration on discrete steps and depended on the tentative trial-and-error choice of a safe dwell temperature. In order to get a more complete picture, and following the work of Struzziero and Skordos,[3] we decided to determine the Pareto optimal front using multi-objective genetic algorithm optimization and compare it with the results of the previous optimization, for the processing of 8, 16 and 24 mm composites. We did not alter the heating and cooling rates of the preheating step, which were fixed at 5 ºC/min and we did not change the final dwell temperature, which was kept at 120 ºC. The range of first dwell temperatures was also limited depending on the

sample thickness. Table 11 shows the different constraints for the variables T_{dwell}, t_{dwell}, $\Delta T_{preheat}(= T_{preheat} - T_{dwell})$ and β. The parameters of the genetic algorithm are shown in Table 2. Convergence of the front was achieved in a reduced number of generations, as reported in the literature [3]. The results in Figure 14 clearly show the effect of composite thickness on processing time and quality. The Pareto front is shifted to longer curing times and higher values of $S_{x,mean}$ when the composite thickness increases. The Pareto-optimal fronts have two clearly distinct regions. For shorter curing cycles, there is a drastic decrease in $S_{x,mean}$ with increasing t_{cycle}, while after certain threshold value, further improvement in quality requires exceedingly long curing cycles. Therefore, an optimum trade-off between quality and processing time can be found in the region before the plateau in quality at longer processing times. Upon examination of the parameters of the curing cycles of the Pareto front, it is generally observed that higher quality requires lower T_{dwell}, longer t_{dwell} and smaller β. Increasing thickness requires further lowering of T_{dwell}, longer t_{dwell} and smaller β. There is not a very strong influence of composite thickness on the value of $T_{preheat}$, which was quite similar to the value of 70 ºC that was determined in the previous optimization. These trends agree well with the values reported in Table 10.

Figure 14

Table 11

Given the upper and lower bounds of the adjustment parameters in Table 11, it cannot be guaranteed that the condition $T > T_g(x)$ was fulfilled for all the simulations carried out throughout the optimization procedure. However, it was verified that $T > T_g(x)$ for all the points in the Pareto fronts of the 8, 16 and 24 mm composite parts, except for the point with the highest $S_{x,mean}$ (poorest quality) and shortest t_{cycle} in the Pareto front of the 24 mm composite part. The sets of parameters with exceedingly large $\Delta T_{preheat}$ $(= T_{preheat} - T_{dwell})$ and low T_{dwell}, long t_{dwell}, or very low β, leading to poor quality and/or longer curing cycles, and also producing $T < T_g(x)$ at some point, were naturally excluded from the final solution as a consequence of the evolutionary algorithm employed. Therefore, it can be safely assumed that

optimum curing cycles take place without vitrification and therefore the models used for the thermophysical properties and kinetics are appropriate.

It is noteworthy that the curing programmes determined using the preceding optimization process led to points (green points in Figure 14) very close to the Pareto front, and very close to the change in trend of the Pareto front. From the point of view of processing time, this is a highly optimal situation. Indeed, one can find points in the front with curing parameters very similar to those in Table 10. This is especially true in the case of the 8 and 16 mm composites, but in the case of the 24 mm composite, the optimized is slightly away from the Pareto front. Indeed, it could be found a curing schedule ($T_{dwell} = 33\ ºC$, $T_{preheat} = 73.5\ ºC$, $t_{dwell} = 11.85\ min$, $\beta = 3.13\ ºC/min$) with the same quality but 20 minutes shorter than that shown in Table 10, entry 3. The curing parameters T_{dwell} and $T_{preheat}$ are not that different, but the dwell time t_{dwell} is significantly shortened and the heating rate β is also higher.

The preceding optimization procedure, based on the tentative selection of a safe dwell temperature T_{dwell} and exploration of the decision space in discrete steps, leads to a reasonable trade-off in terms of quality and processing time and near-to-optimal results. However, this may not always provide the best possible solution. The analysis of the Pareto-optimal front provides a more comprehensive picture of the quality/time trade-off and gives the possibility of choosing other curing programmes that meet specific quality/time requirements, without an exceedingly high computational effort. Alternatively, a specific time constraint could be introduced in order to find a single optimum based on weighed multiple objectives, making use of numerical procedures based on evolutionary algorithms, for instance.[9] The same considerations with regards to the choice of quality criteria, the sensitivity of the optimized solution to processing parameters and the control of preparation and processing conditions can be made.

Future prospects

A weak point of the simulations carried out in this work is that the temperature and conversion dependence of the thermal conductivity[1, 3, 8, 24] was not taken into consideration. A comparison with experimental results would obviously lead to discrepancies because of this. However, the results of the simulations clearly show that the concept of sequential heat release (SHR) based on the use of dual-curing formulations can be exploited successfully for the easy control of conversion and temperature profiles. The use of a better model for the thermal conductivity,

taking into account conversion and temperature dependence, would mainly affect the specific values of the cure cycle parameters (T_{dwell}, t_{dwell}, $T_{preheat}$ and β) but the overall picture would not change. Previous reports in the literature [1] make us feel optimistic about that. Work is underway in order to obtain a better description of the thermal conductivity and verify experimentally the predictions of the model in different scenarios. Inverse heat transfer is also a possibility in order to obtain the temperature-conversion dependence of thermal conductivity.[26]

Another shortcoming of the present work is the absence of an analysis of the internal stresses produced during processing.[2] However, as reasoned above, it would not invalidate the concept. Rather, it would only produce solutions somewhat different from those obtained using the fitness function employed in this work, as shown in the literature.[9] The development of internal stresses in optimized and non-optimized systems, and the comparison between simple curing systems and dual-curing systems with SHR could be a matter of future research as well.

The system under study, the off-stoichiometric thiol-epoxy formulation DGS3-0.5, may not be optimal from the point of view of the processing ability, reactivity or material properties. However, such dual-curing systems are highly tailorable. To begin with, both the final material properties and the crosslinking process can be modified by changing the monomer structure and functionality.[12, 13, 35] Replacing the trifunctional thiol by a tetrafuncitonal thiol might increase the $T_{g\infty}$ about 10 ºC, but that would lead to gelation at the end of the first curing stage. In order to be on the safe side, one could additionally reduce the thiol-epoxy ratio to 0.4,[13] which would bring about a number of positive effects: (1) a further increase in $T_{g\infty}$ up to 105 ºC, (2) an ungelled material at the end of the first curing stage, so that crosslinking could take place in the second curing stage and (3) a lower exothermicity during the first curing stage, which would make it much easier to control the exothermicity of the first curing process and therefore the intermediate composite degree of cure. A side negative effect would be that the exothermicity of the second process would increase because of the higher excess of epoxy groups,[12] but the reaction rate would still be low and therefore the crosslinking process could be easily controlled anyway. In addition, one can use other epoxy monomers/resins[35, 42] and change the amount of initiator[19] or type of catalyst[31, 43, 44] to control the reactivity of the curing process. Other dual-curing thermosetting systems such as off-stoichiometric thiol-acrylate[45] or epoxy-amine[46, 47] could be used as well, providing suitable catalysts or initiators were used to activate the curing reactions in a controlled way in order to achieve a sequential heat release (SHR) and therefore

enable easy thermal management during processing. We recently reported a novel off-stoichiometric epoxy-amine system with excellent stability in the intermediate state that could be useful for that purpose.[15, 48]

Given the simulation results and all the above considerations, and in spite of the limitations of the present analysis, we believe that the concept of sequential heat release (SHR), based on dual-curing formulations, could find successful application in the area of composite processing, with plenty of potential research and development ahead.

4 Conclusions

An innovative approach for the control of temperature and conversion profiles during processing of composite parts has been described, making use of the sequential heat release (SHR) concept, based on the use of dual-curing formulations. The methodology outlined in this work exploits some unique features of dual-curing formulations: the occurrence of two consecutive reaction processes with clearly different kinetics, and the control of gelation, and therefore of the intermediate network structure (if any).

The system under study is based on off-stoichiometric thiol-epoxy systems initiated by a nucleophilic tertiary amine. The first reaction taking place, the thiol-epoxy polymerization, is fast and highly exothermic, while the second, the homopolymerization of excess epoxy groups, is considerably slower and less exothermic. The thiol-epoxy ratio has been chosen so that gelation takes place during the second reaction process, so that crosslinking takes place entirely in the second stage of the curing process.

It has been shown that the crosslinking process can be easily controlled if the heat released during the first reaction is effectively dissipated, so that a temperature runaway leading to the premature activation of the second reaction does not occur. It has been found that this can be easily accomplished by selecting a suitable dwell temperature, in order to limit the temperature overshoot due to accumulation of heat within the composite, so that the second reaction is not activated, or at least premature gelation is prevented. Subsequent heating leads to activation of the second reaction and crosslinking, which takes place in a more controlled way due to the reduced remaining exothermicity of the second reaction process. On the basis of this, an easy optimization procedure has been devised leading to shorter processing cycles with highly uniform conversion profiles during the crosslinking stage, for composite parts with thickness of

up to 24 mm. The curing programmes defined on the basis of this procedure are very close to the Pareto-optimal front and represent a reasonable trade-off between quality and processing time.

Due to the tailorability of these systems in terms of material properties, reaction kinetics and network structure build-up, it is envisioned there is a great potential for development in the field. Other dual-curing systems could potentially benefit from this novel processing strategy.

Acknowledgements

The authors would like to thank MINECO (MAT2017-82849-C2-1-R) and Generalitat de Catalunya (2017-SGR-77 and Serra Húnter programme) for the financial support.

References

1 J. L. Bailleul, V. Sobotka, D. Delaunay and Y. Jarny, *Composites Part A: Applied Science and Manufacturing* **34:**695-708 (2003).

2 E. Ruiz and F. Trochu, *Composites Part A: Applied Science and Manufacturing* **36:**806-826 (2005).

3 G. Struzziero and A. A. Skordos, *Composites Part A: Applied Science and Manufacturing* **93:**126-136 (2017).

4 T. A. Gorovaya and V. N. Korotkov, *Composites Part A: Applied Science and Manufacturing* **27:**953-960 (1996).

5 S. R. White and Y. K. Kim, *Composites Part A: Applied Science and Manufacturing* **27:**219-227 (1996).

6 M. Li, Q. Zhu, P. H. Geubelle and C. L. Tucker, *Polymer Composites* **22:**118-131 (2001).

7 N. G. Pantelelis, *Composites Science and Technology* **63:**249-264 (2003).

8 L. Sorrentino and L. Tersigni, *Applied Composite Materials* **19:**31-45 (2012).

9 E. Ruiz and F. Trochu, *Composites Part A: Applied Science and Manufacturing* **37:**913-924 (2006).

10 X. Ramis, X. Fernández-Francos, S. De La Flor, F. Ferrando and À. Serra, Click-based dual-curing thermosets and their applications (chapter 16), in *Thermosets 2nd edition: Structure, Properties and Application*, ed by Q. Guo. Elsevier (2017).

11 J. Studer, C. Dransfeld and K. Masania, *Composites Part A: Applied Science and Manufacturing* **87:**282-289 (2016).

12 X. Fernandez-Francos, A.-O. Konuray, A. Belmonte, S. De la Flor, A. Serra and X. Ramis, *Polymer Chemistry* **7:**2280-2290 (2016).

13 A. Belmonte, X. Fernàndez-Francos, À. Serra and S. De la Flor, *Materials & Design* **113:**116-127 (2017).

14 R. A. Venditti and J. K. Gillham, *Journal of Applied Polymer Science* **64:**3-14 (1997).

15 N. Areny, O. Konuray, X. Fernàndez-Francos, J. M. Salla, J. M. Morancho and X. Ramis, *Thermochimica Acta* **666:**124-134 (2018).

16 X. Fernández-Francos and X. Ramis, *European Polymer Journal* **70:**286-305 (2015).

17 X. Fernandez-Francos, W. D. Cook, J. M. Salla, A. Serra and X. Ramis, *Polymer International* **58:**1401-1410 (2009).

18 *Recommended reference materials for the realization of physicochemical properties*, Blackwell Scientific Publications (1985).

19 A. O. Konuray, X. Fernandez-Francos and X. Ramis, *Polymer Chemistry* **8:**5934-5947 (2017).

20 Y. Nawab, X. Tardif, N. Boyard, V. Sobotka, P. Casari and F. Jacquemin, *Composites Science and Technology* **73:**81-87 (2012).

21 J. P. Pascault, H. Sautereau, J. Verdu and R. J. J. Williams, *Thermosetting polymers*, Marcel Dekker, New York [etc.] : (2002).

22 X. Fernandez-Francos, X. Ramis and A. Serra, *Journal of Polymer Science Part A: Polymer Chemistry* **52:**61-75 (2014).

23 D. W. Van Krevelen, *Properties of polymers : their correlation with chemical structure, their numerical estimation and prediction from additive group contributions / by D.W. van Krevelen* (1990).

24 N. Boyard, A. Millischer, V. Sobotka, J. L. Bailleul and D. Delaunay, *Composites Science and Technology* **67:**943-954 (2007).

25 U. Hammerschmidt and V. Meier, *International Journal of Thermophysics* **27:**840-865 (2006).

26 A. A. Skordos and I. K. Partridge, *Inverse Problems in Science and Engineering* **12:**157-172 (2004).

27 P. I. Karkanas and I. K. Partridge, *Journal of Applied Polymer Science* **77:**1419-1431 (2000).

28 S. Vyazovkin and N. Sbirrazzuoli, *Macromolecular Rapid Communications* **27:**1515-1532 (2006).

29 S. Vyazovkin, *Journal of Computational Chemistry* **18:**393-402 (1997).

30 L. A. Pérez-Maqueda and J. M. Criado, *Journal of Thermal Analysis and Calorimetry* **60:**909-915 (2000).

31 R. M. Loureiro, T. C. Amarelo, S. P. Abuin, E. R. Soulé and R. J. J. Williams, *Thermochimica Acta* **616:**79-86 (2015).

32 X. Fernandez-Francos, W. D. Cook, A. Serra, X. Ramis, G. G. Liang and J. M. Salla, *Polymer* **51:**26-34 (2010).

33 X. Fernandez-Francos, *European Polymer Journal* **55:**35-47 (2014).

34 A. Belmonte, G. C. Lama, G. Gentile, P. Cerruti, V. Ambrogi, X. Fernández-Francos and S. De la Flor, *European Polymer Journal* **97:**241-252 (2017).

35 A. Belmonte, C. Russo, V. Ambrogi, X. Fernández-Francos and S. De la Flor, *Polymers* **9:**113 (2017).

36 D. Guzmán, X. Ramis, X. Fernández-Francos and A. Serra, *European Polymer Journal* **59:**377-386 (2014).

37 S. K. Ooi, W. D. Cook, G. P. Simon and C. H. Such, *Polymer* **41:**3639-3649 (2000).

38 B. A. Rozenberg, *Advances in Polymer Science* **75:**113-165 (1986).

39 K. J. Ivin, in *Polymer Handbook*, ed by J. Brandrup and E. H. Immergut. Wiley, New York (1975).

40 A. Hale, C. W. Macosko and H. E. Bair, *Macromolecules* **24:**2610-2621 (1991).

41 E. Frulloni, M. M. Salinas, L. Torre, A. Mariani and J. M. Kenny, *Journal of Applied Polymer Science* **96:**1756-1766 (2005).

42 D. Guzmán, X. Ramis, X. Fernández-Francos and A. Serra, *Polymers* **7:**680-694 (2015).

43 K. Jin, W. H. Heath and J. M. Torkelson, *Polymer* **81:**70-78 (2015).

44 A. O. Konuray, X. Fernández-Francos and X. Ramis, *Polymer* **116:**191-203 (2017).

45 D. P. Nair, N. B. Cramer, J. C. Gaipa, M. K. McBride, E. M. Matherly, R. R. McLeod, R. Shandas and C. N. Bowman, *Advanced Functional Materials* **22:**1502-1510 (2012).

46 X. Fernandez-Francos, D. Santiago, F. Ferrando, X. Ramis, J. M. Salla, À. Serra and M. Sangermano, *Journal of Polymer Science Part B: Polymer Physics* **50:**1489-1503 (2012).

47 J. M. Morancho, X. Ramis, X. Fernández-Francos, J. M. Salla, A. O. Konuray and À. Serra, *Journal of Thermal Analysis and Calorimetry* **133:**519-527 (2018).

48 A. O. Konuray, N. Areny, J. M. Morancho, X. Fernández-Francos, À. Serra and X. Ramis, *Polymer* **146:**42-52 (2018).

TABLES

Table 1: Notation and composition of the formulations studied in this work, in weight fraction (wt.%). It is also included the thiol:epoxy molar ratio (r)

Formulation	r	$wt.\%$ $1MI$	$wt.\%$ $DGEBA$	$wt.\%$ $S3$
DGS3-1	1	0.99	56.18	42.83
DGS3-0.5	0.5	0.99	71.68	27.33

Table 2: MATLAB parameters for the genetic-algorith multiobjective optimization.

Parameter	*Value*
Population size	60
Population type	Double vector (constraint dependent)
Selection function	Tournament (size = 2)
Crossover fraction	0.5
Crossover function	Intermediate (ratio = 1)
Mutation function	Constraint dependent
Pareto front population fraction	0.8
Maximum number of generations	15

Table 3: Summary of the calorimetric analysis of the DGS3-1 and DGS3-0.5 formulations

	DGS3-1	DGS3-0.5
$\Delta h\ or\ \Delta h_1\ (J/g)$	419	279
$\Delta h\ or\ \Delta h_1\ (kJ/ee)$	128	134
$\Delta h_2\ (J/g)$	-	193
$\Delta h_2\ (kJ/ee)$	-	93
T_{g0} (°C)	-46.5	-36.6
$\Delta c_{p0}\ (J/g \cdot K)$	0.56	0.55
T_{gint} (°C)	-	9.5
$\Delta c_{pint}\ (J/g \cdot K)$	-	0.55
$T_{g\infty}$ (°C)	34	79
$\Delta c_{p\infty}\ (J/g \cdot K)$	0.45	0.41
$x_{epoxy,gel}$	0.80	0.63

Table 4: Kinetic parameters of the curing of DGS3-1 formulation.

Induction (eq. (14))	$E_{ind}(kJ/mol)$	58.94	
	$g(x_{ind})/k_{0,ind}\ (s)$	-14.83	
Rate equation (eq. (8))		$i = 1$	$i = 2$
	$E_i(kJ/mol)$	56.59	62.54
	$ln(k_{0,i})\ (s^{-1})$	15.76	16.89
	m_i	1.558	0.808
	n_i	0.984	3.486

Table 5: Kinetic parameters of the first curing process of DGS3-0.5 formulation.

Induction (eq. (14))	$E_{ind}(kJ/mol)$	58.32	
	$g(x_{ind})/k_{0,ind}\ (s)$	-15.17	
		$i=1$	$i=2$
Rate equation (eq. (8))	$E_i(kJ/mol)$	61.23	61.70
	$ln(k_{0,i})\ (s^{-1})$	18.20	17.55
	m_i	3.675	0.988
	n_i	0.762	1.043

Table 6: Kinetic parameters of the second curing process of DGS3-0.5 formulation.

Induction (eq. (14))	$E_{ind}(kJ/mol)$		43.15	
	$g(x_{ind})/k_{0,ind}\ (s)$		-10.23	
		$i=1$	$i=2$	$i=3$
Rate equation (eq. (8))	$E_i(kJ/mol)$	81.39	42.44	53.73
	$ln(k_{0,i})\ (s^{-1})$	19.26	8.24	16.00
	m_i	0.002	1.242	3.115
	n_i	3.385	1.692	9.092

Table 7: Relative error associated with the determination of the induction time parameters and the parameters of the rate curves.aThe error associated with the determination of the induction time has been determined on the basis of the calculated and experimental induction time for the isothermal experiments.

	Induction time[a]	Rate curves (eq (9))
DGS3-1	0.036	0.044
DGS3-0.5 1st process	0.017	0.046
DGS3-0.5 2nd process	0.31	0.068

Table 8: Expressions for the temperature dependence of the specific heat capacities (c_p, in $kJ/kg \cdot K$) of the uncured, intermediate and cured materials (above their glass transition) and the temperature dependence of the densities (ρ, in kg/m^3) of the uncured, intermediate and cured materials (above their glass transition). The values of the thermal conductivity of the fully cured material (λ_r, in $W/m \cdot K$) are also shown. Room temperature T_0 was equal to 20 ºC for the measured densities.

	DGS3-1	DGS3-0.5
$c_{p0}\ (T)$	$1723.8 + 1.8401 \cdot T$	$1732.0 + 2.2367 \cdot T$
$c_{pint}\ (T)$	-	$1662.2 + 1.7565 \cdot T$
$c_{p\infty}\ (T)$	$1698.7 + 1.7807 \cdot T$	$1723.8 + 1.6761 \cdot T$
$\rho_0\ (T)$	$\frac{1194}{1 + 0.625 \cdot 10^{-3} \cdot (T - 20)}$	$\frac{1183}{1 + 0.625 \cdot 10^{-3} \cdot (T - 20)}$
$\rho_{int}\ (T)$	-	$\frac{1202}{1 + 0.625 \cdot 10^{-3} \cdot (T - 20)}$
$\rho_\infty\ (T)$	$\frac{1230}{0{,}000573 \cdot T + 0.988537}$	$\frac{1221}{0{,}000514 \cdot T + 0.974777}$
λ_r	0.1996	0.1858

Table 9: Summary of the original runs of dual-curing system DGS3-0.5 and their main parameters.

Entry	L (mm)	T_{dwell} $(ºC)$	t_{dwell} (min)	β $(ºC/min)$	$S_{x,mean}$	t_{cycle} (min)
1	8	80	6.67	5	0.0234	64.6
2	8	70	10	5	0.0060	69.1
3	8	60	16.67	5	0.0012	75.9
4	16	45	55	5	0.0045	112.8
5	24	35	110	5	0.0122	167.1

Table 10: Summary of the optimized runs optimized for preheat, dwell time and heating rate.

Entry	L (mm)	T_{dwell} $(ºC)$	$T_{preheat}$ $(ºC)$	t_{dwell} (min)	β $(ºC/min)$	$S_{x,mean}$	t_{cycle} (min)
1	8	60	70	5	4	0.0014	70.5
2	16	45	70	11.7	3.5	0.0028	84.9
3	24	35	70	28.3	2.5	0.0042	112.9

Table 11: Constraints used for the determination of the Pareto-optimal front.

Parameter	*L=8 mm*	*L=16 mm*	*L=24 mm*
T_{dwell} $(ºC)$	30-90	25-70	25-50
t_{dwell} (min)	0-120	0-180	0-240
$\Delta T_{preheat}$ $(ºC)$	0-60	0-60	0-60
β $(ºC/min)$	0.1-5	0.1-5	0.1-5

FIGURE CAPTIONS

Scheme 1: From left to right, general representation of dual-curing processing, processing requirements for the present application and dual-curing reactive system employed.

Figure 1: (a) Discretization of the composite part (the dots indicate the position of the nodal temperatures) and (b) programming of the curing schecule.

Figure 2: Comparison of the dynamic curing at 10 ºC/min of formulations DGS3-1 and DGS3-0.5. The inset shows in detail the curing rate for the second stage of the DGS3-0.5 formulation.

Figure 3: Comparison of the isothermal curing (dx/dt) for the 1st (above) and 2nd (below) processes of the curing of DGS3-0.5 formulation. Samples for the study of the 2nd curing process were pre-cured at 80 ºC in the DSC up to the point when the 1st curing process was finished.

Figure 4: Comparison of the experimental and modelled reaction rate (dx/dt) (upper graph) and reaction time (lower graph) for the 1st process of the curing of DGS3-0.5 formulation under isothermal conditions.

Figure 5: Simulation of conversion and temperature profiles of 8 mm composite parts of formulation DGS3-1 and DGS3-0.5 with 50 % volume fraction of filler, at a first dwell temperature of 70 ºC. The dotted lines in the temperature plot represent the programming temperature.

Figure 6: Conversion profiles (left graph) and temperature profiles (right graph) of 8 mm composite parts of formulation DGS3-1 with 50 % volume fraction of filler, at a first dwell temperature of 70 ºC. The dotted lines represent on the conversion graph represents the conversion at gelation. 21 nodes, representing half of the composite thickness (central node = 1, surface node = 21), have been employed in this representation.

Figure 7: Conversion profiles (left graph) and temperature profiles (right graph) of 8 mm composite parts of formulation DGS3-0.5 with 50 % volume fraction of filler, at a first dwell temperature of 70 ºC. The dotted lines represent on the conversion graph represents the conversion at gelation. 21 nodes, representing half of the composite thickness (central node = 1, surface node = 21) , have been employed in this representation.

Figure 8: Simulation of conversion and temperature profiles of 8 mm composite parts of formulation DGS3-0.5 with 50 % volume fraction of filler, at at a first dwell temperatres of 60, 70 and 80 ºC. The dotted lines in the temperature plot represent the programming temperature.

Figure 9: Simulation of conversion and temperature profiles of 8 mm, 16 mm and 24 mm composite parts of formulation DGS3-0.5 with 50 % volume fraction of filler, at a first dwell temperature of 60 ºC (8 mm) 45 ºC (16 mm) and 35 ºC (24 mm), without any optimization.

Figure 10: Optimization of cycle parameters (dwell time, second heating rate) for the curing of 16 mm composite parts of formulation DGS3-0.5 with 50 % volume fraction of filler, at a first dwell temperature of 45 ºC and different dwell times and 2nd heating rates.

Figure 11: Simulation of conversion and temperature profiles of 16 mm composite parts of formulation DGS3-0.5 with 50 % volume fraction of filler, at a first dwell temperature of 45 ºC, original and optimized curing programmes. The dotted lines in the temperature plot represent the programming temperature.

Figure 12: Optimization of cycle parameters (dwell time, preheat peak temperature) for the curing of 16 mm composite parts of formulation DGS3-0.5 with 50 % volume fraction of filler, at a first dwell temperature of 45 ºC and preheat peak temperatures, with a fixed second heating rate of 3.5 ºC/min.

Figure 13: Simulation of conversion and temperature profiles of 8 mm, 16 mm and 24 mm composite parts of formulation DGS3-0.5 with 50 % volume fraction of filler, at a first dwell temperature of 60 ºC (8 mm) 45 ºC (16 mm) and 35 ºC (24 mm), optimized for preheating, dwell time and second heating rate. The dotted lines in the temperature plot represent the programming temperature.

Figure 14: Determination of the Pareto-optimal fronts for the processing of 8, 16 and 24 mm thick composites and comparison with the previously optimized points (entries 1, 2 and 3 in Table 10). The lines have been drawn to guide the eye.

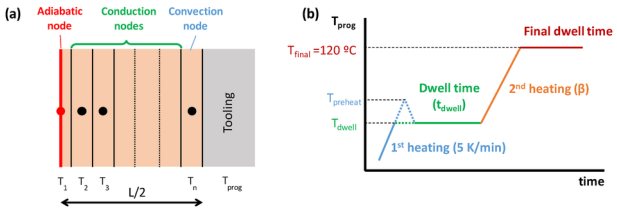

PI_5743_Figure 1.tif

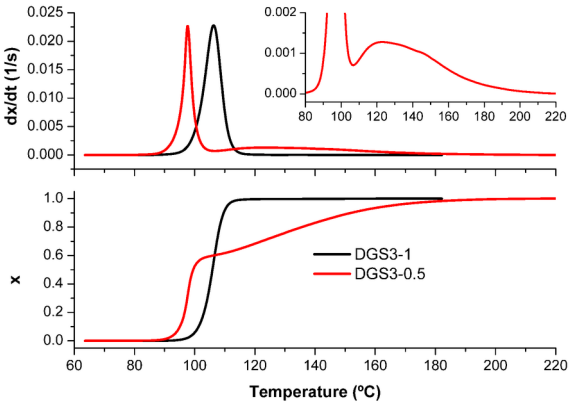

PI_5743_Figure 2.tif

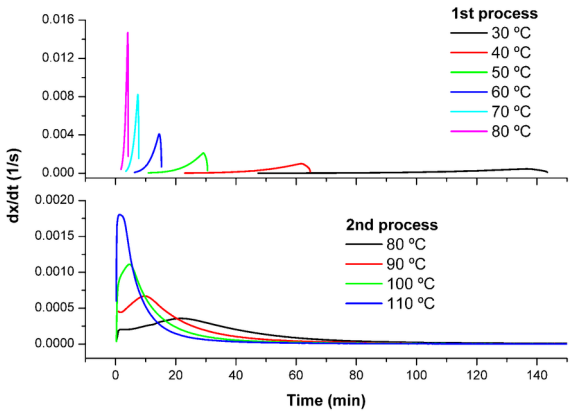

PI_5743_Figure 3.tif

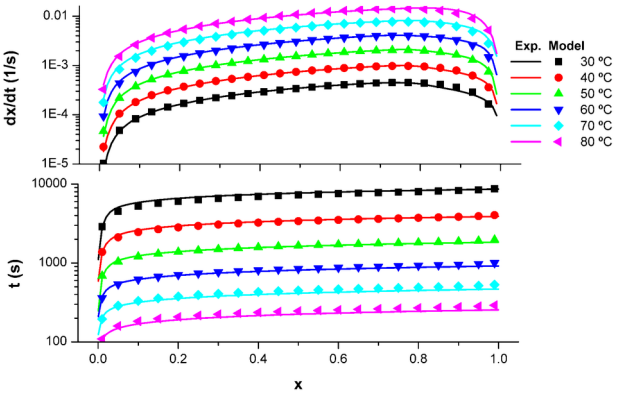

PI_5743_Figure 4.tif

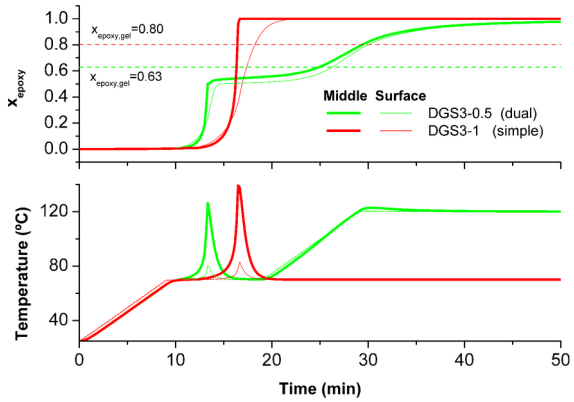

PI_5743_Figure 5.tif

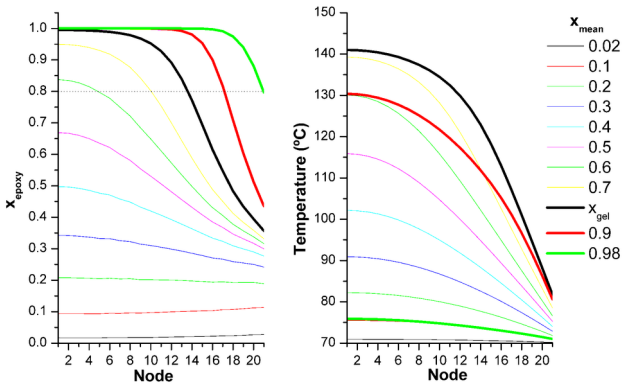

PI_5743_Figure 6.tif

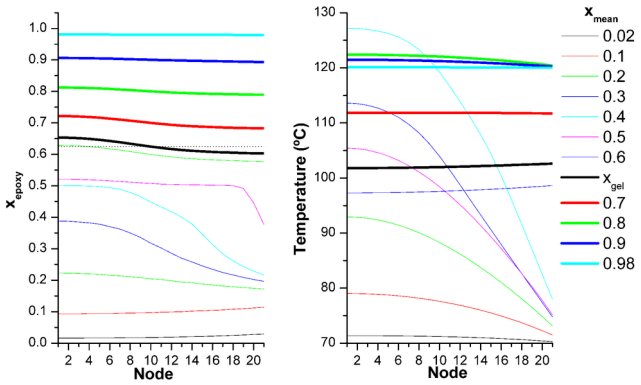

PI_5743_Figure 7.tif

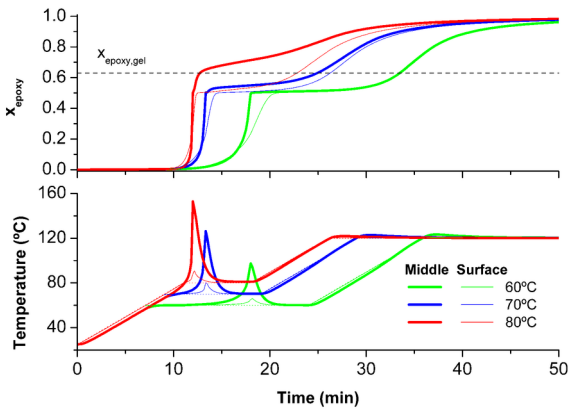

PI_5743_Figure 8.tif

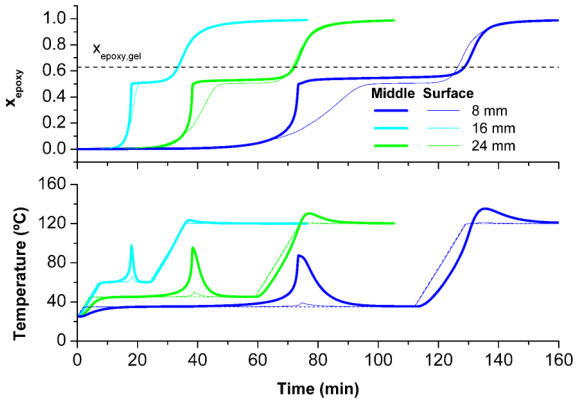

PI_5743_Figure 9.tif

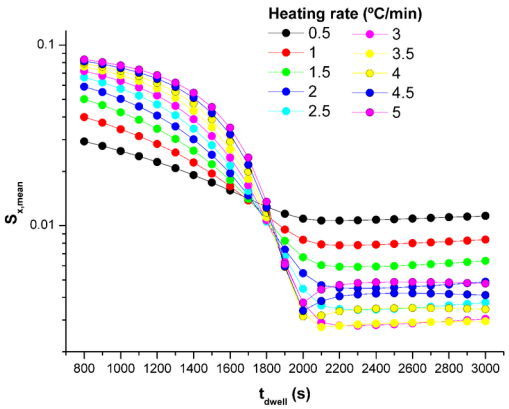

PI_5743_Figure 10.tif

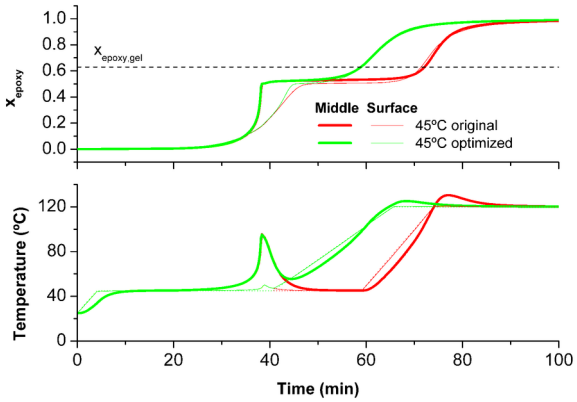

PI_5743_Figure 11.tif

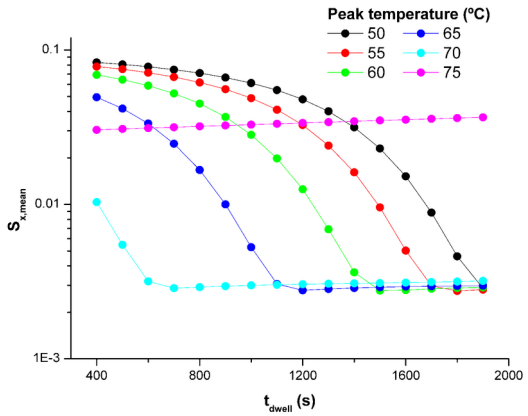

PI_5743_Figure 12.tif

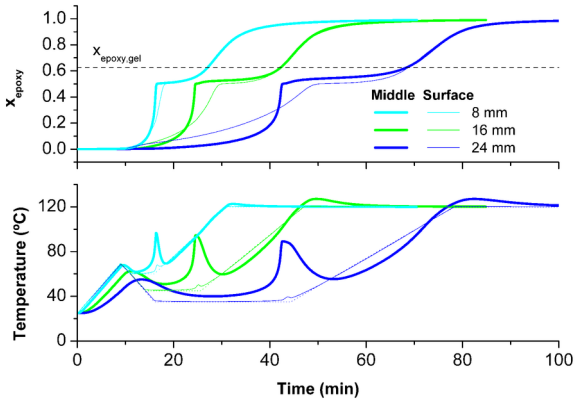

PI_5743_Figure 13.tif

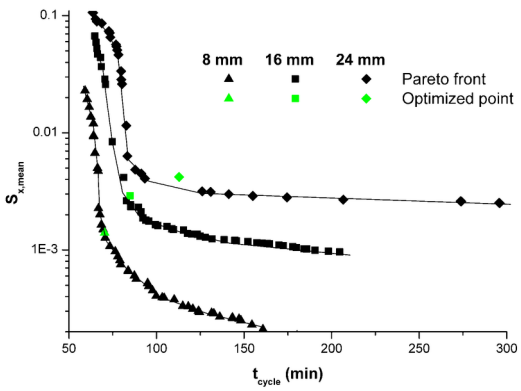

PI_5743_Figure 14.tif

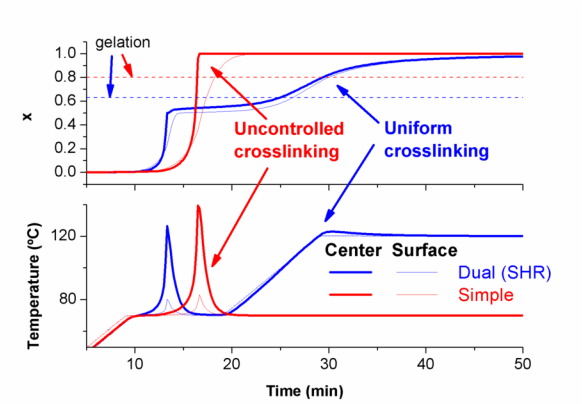

PI_5743_Graphical figure.tif

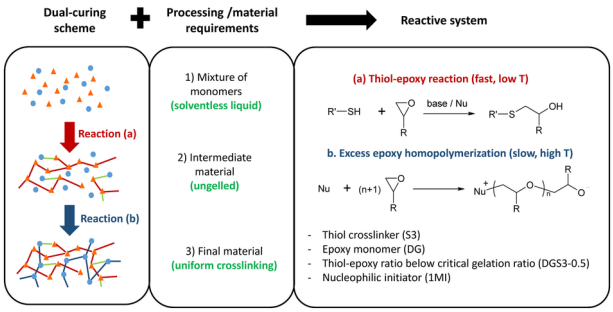

PI_5743_Scheme 1 new.tif